scientific reports

Check for updates

OPEN

Entropy and seasonal isotopic duality reveal the sustainability paradox of the upper Ganga River

Manish Kumar[1,2,8]✉, Sachin Tripathi[1,2,8], Rajesh Singh[3]✉, Shive Prakash Rai[4], Nilotpal Das[5], Vivek Agarwal[6], Pawan Kumar Jha[7] & Juan Antonio Torres-Martinez[1]

Mountain headwaters are widely regarded as pristine reference systems; however, mounting evidence reveals that even these fragile environments are no longer insulated from the pervasive influence of the Anthropocene. We investigated the seasonal variations in hydrogeochemical signatures and isotopic duality ($\delta^{18}O$, δD) along a 255-km stretch of the upper Ganga River (Gangotri to Haridwar) during monsoon and post-monsoon seasons, using a spatially resolved, process-focused dataset. Our integrative approach incorporated analysis of geogenic structures, anthropogenic influences, entropy-based water quality indices (EWQI), and multivariate statistical evaluations. The findings demonstrate a marked isotopic and hydrogeochemical duality during the monsoon, which diminishes post-monsoon as water chemistry becomes increasingly homogenized through the mixing and buffering of residual monsoon runoff, stored meltwater, and groundwater contributions. This process results in dilute HCO_3^-–Ca^{2+}–Mg^{2+} waters characterized by a weaker geochemical structure but elevated concentrations of diffuse anthropogenic tracers; namely NO_3^-, K^+, and Cl^-. Post-monsoon, reduced discharge and a greater contribution from groundwater induce stronger geogenic structuring; isotopic signatures cluster sequentially through pH and total suspended solids (TSS) before ion compositions, and hydrochemistry transitions toward HCO_3^-–SO_4^{2-}–Ca^{2+}–Mg^{2+} facies with downstream Na^+–Cl^- enrichment. The EWQI classified > 50% of samples as 'very poor', with deterioration more pronounced in the post-monsoon. Together, these findings highlight a sustainability paradox that sacred glacier-fed headwaters, commonly treated as pristine baselines in policy frameworks, already carry detectable anthropogenic signals, with implications for monitoring and governance aligned with Sustainable Development Goal 6 (Clean Water and Sanitation).

Rivers sustain ecosystems, economies, and cultures, while regulating the transfer of freshwater, sediments, solutes, and nutrients from continents to oceans[1–4]. However, riverine environments are increasingly challenged by the combined effect of anthropogenic pollution, climate change, and land use pressures, which together compromise water security functions and ecosystem integrity[3–6]. Because river chemistry integrates upstream geogenic processes with cumulative human influences, headwater and mountain-front reaches exert a disproportionate control over downstream water quality baselines and on the propagation of contaminant signals through a basin[1,7,8]. Himalayan rivers are particularly informative in this regard, originating in comparatively pristine cryospheric settings yet rapidly transitioning into densely populated, intensively landscapes where hydrology and water quality respond to strong seasonal forcing and accelerating development[9,10].

Across South Asia, many glacial-fed river systems traditionally considered as perennial are now under growing stress from rapid urbanization, expanding infrastructure, and intensified agriculture, superimposed on changing hydroclimatic conditions[11–13]. Within this regional context, the Ganga River floodplains (GRF) represent one of the most important socio-hydrological systems in the Indian sub-continent[14]. The Ganga River, among the largest river systems globally, is both hydrologically essential and culturally iconic. It originates from the Gangotri glacier (approx. 4000 m a.s.l.) in Uttarakhand, India, descends through steep Himalayan valleys,

[1]Escuela de Ingeniería y Ciencias, Tecnologico de Monterrey, Ave. Eugenio Garza Sada 2501, 64700 Monterrey, NL, Mexico. [2]Sustainability Cluster, School of Advanced Engineering, UPES, Dehradun, Uttarakhand 248007, India. [3]Environmental Hydrology Division, National Institute of Hydrology, Roorkee, Uttarakhand 247667, India. [4]Department of Geology, Banaras Hindu University, Varanasi 221005, India. [5]Encore Insoltech Private Ltd, Randesan, Gandhinagar, Gujarat, India. [6]Science and Environment, Northumbria University, Newcastle, UK. [7]Centre of Environmental Studies, University of Allahabad, Prayagraj, Uttar Pradesh 211002, India. [8]Manish Kumar and Sachin Tripathi contributed equally to this work. ✉email: manish@tec.mx; manish.env@gmail.com; rsingh.nih@gmail.com

and enters the Indo-Gangetic Plain[15]. Along its course, the river provides water to nearly 500 million people and supports agricultural, industrial, and domestic needs, as well as religious and spiritual practices[14,16,17]. Despite its glacial origin, the river is subject to substantial anthropogenic pressures as it traverses pilgrimage centers, expanding towns, and agricultural landscapes. These pressures are further compounded by climate change, which is altering cryospheric melt contributions and modulating the intensity and timing of the South Asian monsoon[18], thereby reshaping dilution capacity, solute transport, and contaminant mobility.

A process-based understanding of the hydrochemistry and isotope systematics is therefore central to diagnosing water quality evolution of Himalayan rivers. Hydrochemical facies capture the integrated effects of carbonate and silicate weathering, sulfide oxidation, and ion exchange, and groundwater-surface water interactions[19,20], while stable water isotopes ($\delta^{18}O$, δD) provide diagnostic insights into water sources, mixing proportions, residence times, and evaporative effects[21–23]. In monsoon-driven basins, intensified hydrologic variability controls discharge and connectivity across hillslopes, aquifers, and river channels, strongly influencing the mobilization, transport, and attenuation of both solutes and contaminants[24]. Monsoon-driven fluctuations also affect agricultural productivity, irrigation demands, alter return flows and shifting the balance between surface and groundwater systems[20]. The primary water sources for the Ganga River and its tributaries include baseflow (groundwater), and snow or ice melt, with groundwater contributing about 23% of total flow, emphasizing the need to interpret river chemistry within a coupled surface-subsurface framework[25]. Together, hydrochemistry and isotopes provide a robust lens to disentangle geogenic and anthropogenic controls on river chemistry and to identify how these signals strengthen or weaken across seasons.

Comparative evidence from across the Indian subcontinent further highlights that the expression of anthropogenic signatures is strongly influenced by lithology and land-use intensity. Recent tracer-informed and hydrogeochemical assessments in contrasting Indian terrains[6] spanning humid tropical critical zones, densely populated urban–agricultural mosaics, and Himalayan foreland settings[17], show that differences in bedrock composition, weathering pathways, and human pressures can shift both background geochemical baselines and the magnitude and composition of pollution signals[6,17]. Studies from tropical hard-rock critical zones of the Western Ghats highlight how monsoon-driven erosion, agrochemical inputs, and lithological weathering jointly shape seasonal tracer responses[18]. Such comparative context is essential for interpreting the upper Ganga, where carbonate–silicate transitions, steep relief, and rapid downstream changes in land use create pronounced spatial gradients in hydrochemical behaviour and vulnerability.

Seasonality is a defining control on large river dynamics in South Asia. The alternation between intense monsoon rainfall and comparatively arid winter conditions governs discharge, residence times, and geochemical processing, thereby shaping nutrient cycling, sediment transport, and contaminant dispersion[15,26]. Seasonality also modulates habitat connectivity and ecological function, while simultaneously interacting with socio-economic pressures (e.g., pilgrimage fluxes, urban water demand, and seasonal irrigation), producing complex coupled human-natural responses that can amplify water quality deterioration during low-flow periods.

Beyond classical hydrochemistry, entropy-based approaches provide a complementary lens for synthesizing multivariate water quality information and diagnosing disturbance. The entropy-based water quality index (EWQI) integrates multiple chemical parameters with weights derived from their informational content, enabling a quantitative assessment that is sensitive to both concentration changes and the increased disorder introduced by anthropogenic disturbance[27,28]. In thermodynamic terms, rivers behave as dissipative systems: high flows can temporarily reduce apparent disorder through dilution and flushing, whereas low flows can enhance the accumulation of entropy associated with pollutant loading, suspended matter, and reduced assimilative capacity. Applying entropy-based metrics to Himalayan river corridors, therefore offers a structured way to link hydrochemistry, seasonality, and human pressures within a sustainability-science framework.

The upper Ganga, spanning Gangotri to Haridwar, provides a strategically important natural laboratory to examine the seasonal interplay of geogenic structuring and anthropogenic imprinting. This ~ 255 km reach spans glacial headwaters, steep Himalayan valleys, the Bhagirathi–Alaknanda confluence at Devprayag, and the entry into the Indo-Gangetic Plain at Haridwar (Fig. 1). It also intersects pilgrimage centres, expanding settlements, agriculture, and point-source and diffuse effluent pathways[29,30]. By integrating hydrogeochemical facies, isotopic tracers, statistical analyses, and EWQI, this study aims to (i) characterize seasonal duality in hydrochemistry and isotopes, (ii) disentangle geogenic versus anthropogenic contributions, (iii) interpret water quality deterioration using entropy perspectives, and (iv) develop an integrated framework for assessing hydrochemistry and human impacts along the upper Ganga River.

The novelty lies in its integrated framework that introduces entropy-based water quality assessment to diagnose system-level disorder in Upper Ganga headwaters and systematically characterizes seasonal isotopic clustering pathways revealing mechanistic transitions from buffering to baseflow-integrated controls. Additionally, this study provides direct evidence of anthropogenic signatures even in glacial source zones traditionally assumed pristine and quantitatively demonstrates that monsoon dilution masks chronic pressures that re-emerge during baseflow. These advances carry critical implications for Sustainable Development Goal 6 (Clean Water and Sanitation) aligned monitoring and governance frameworks.

Results and discussion

Geological and hydrological controls

The hydrogeochemical evolution of the upper Ganga River is primarily controlled by the coupled effects of bedrock lithology and a strong seasonal hydrological regime. The sampling transect (Fig. 1a–d) crosses (i) crystalline gneisses and granites in the Gangotri headwaters, (ii) carbonate-bearing metasediments at midstream, and (iii) progressively more extensive alluvial deposits toward Haridwar. This lithological transition provides a first-order explanation for the systematic downstream enrichment in dissolved ions (Supplementary Table S1). Headwaters at Gangotri (G1, elevation > 3000 m) are weakly mineralized, with electrical conductivity (EC)

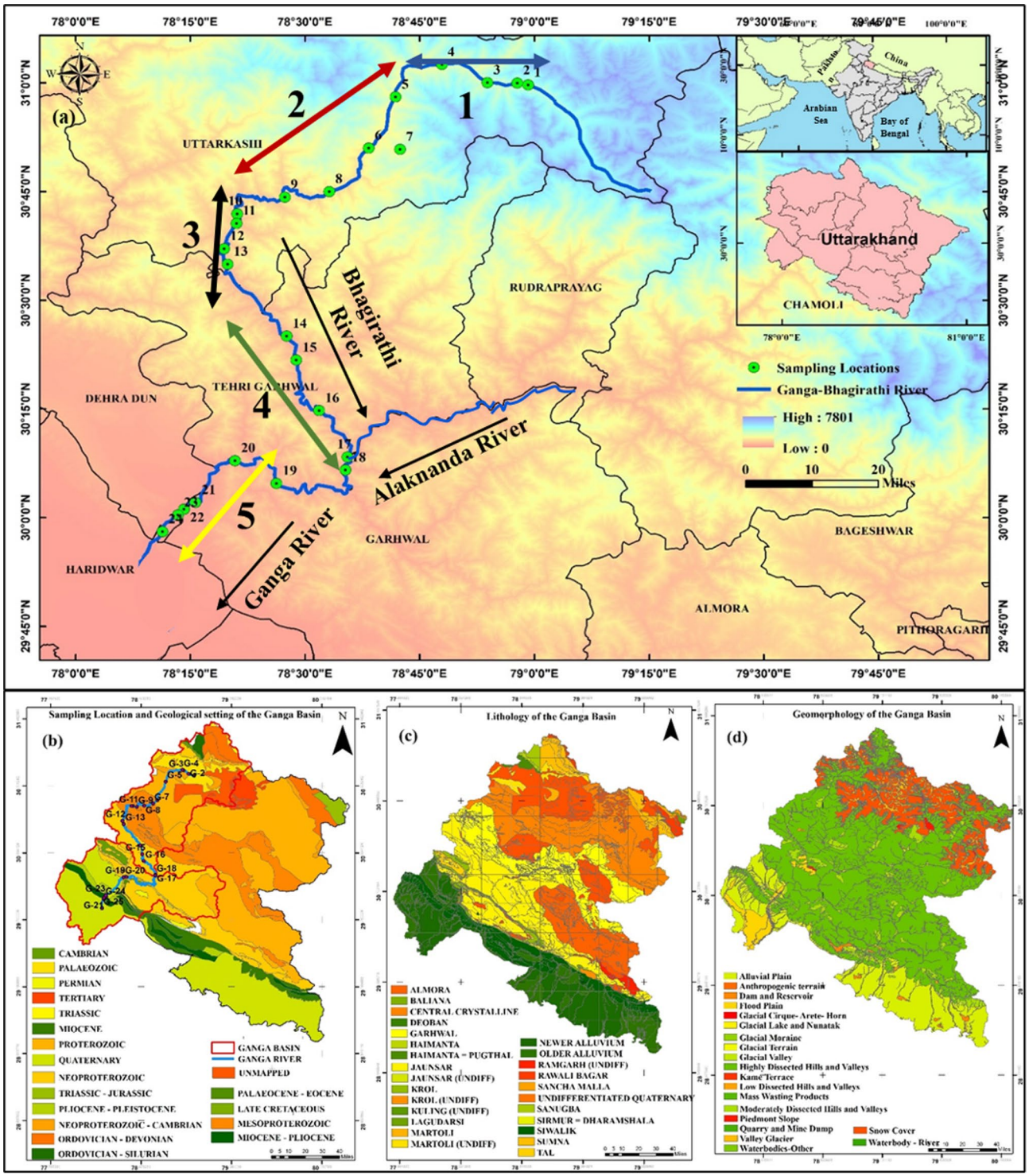

Fig. 1. Sampling sites and geomorphic context of the upper Ganga River. Transect from Gangotri (3143 m.a.s.l.) to Haridwar (255 km downstream), showing (**a**) sampling location, (**b**) geological setting, (**c**) lithology, and (**d**) geomorphology. The maps illustrate how glacial headwaters, carbonate–silicate bedrock transitions, and alluvial plains frame the hydrochemical template upon which seasonal and anthropogenic processes act.

values below 120 µS cm^{-1} (Table S1) and dominated by Ca^{2+} and HCO_3^- (Fig. 2iii). As the river descends, EC increases up to 538 µS cm^{-1} at Haridwar (G23), reflecting increased solute acquisition from carbonate-bearing lithologies and additional inputs from human activities in the densely occupied downstream corridor.

Seasonal discharge variability imposes a clear secondary control by modulating dilution, residence time, and the relative contribution of groundwater (baseflow). During the monsoon, high discharge promotes dilution

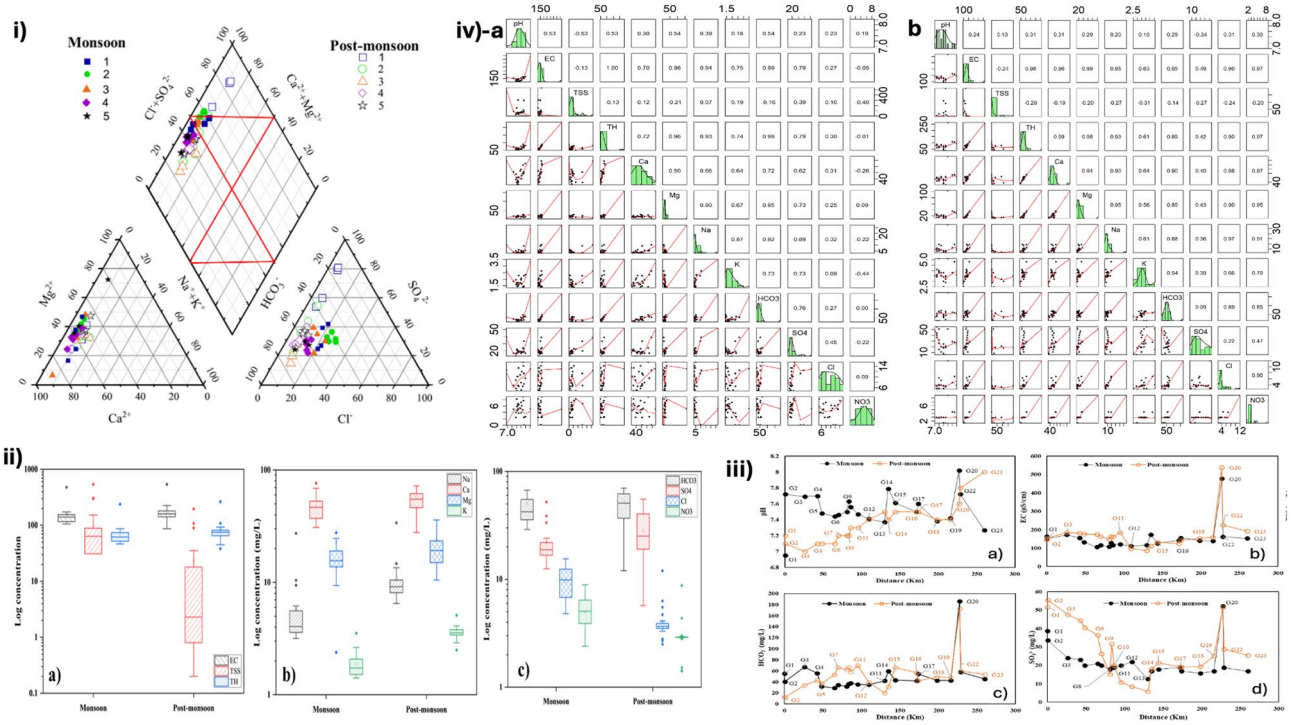

Fig. 2. Seasonal hydrochemistry of the upper Ganga reveals monsoon dilution and post-monsoon solute enrichment. (**i**) Piper plots showing hydrochemical facies shifts. (**ii**) Box plots (a–c) summarizing seasonal variability in key parameters. (**iii**) Longitudinal trends of panels (a–d) for pH, EC, HCO_3^-, and SO_4^{2-} (iv) Pearson correlation coefficients for (a) monsoon, and (b) post-monsoon.

of dissolved constituents, resulting in lower EC values (mean 153 µS cm^{-1}). By comparison, post-monsoon conditions are characterized by reduced flows, longer effective residence times, and greater baseflow influence, leading to solute concentration and higher EC values (mean 175 µS cm^{-1}). This seasonal contrast confirms hydrological regulation of ionic strength superimposed on the lithological template. Total hardness (TH) and the principal alkaline earths (Ca^{2+} and Mg^{2+}) increase downstream in both seasons (Fig. S1), supporting persistent carbonate weathering as the dominant geogenic driver. Notably, post-monsoon concentrations are systematically higher, consistent with enhanced groundwater contributions and increased water-rock interaction under low-flow conditions.

Superimposed on these natural controls, localized post-monsoon enrichments in Na^+, K^+, SO_4^{2-}, Cl^-, and NO_3^-, particularly near Saptrishi Ashram (G20), indicate the strengthening of anthropogenic signals when assimilative capacity is lowest.This condition is also attributed to the diversion of the river upstream for a run-of-the-river hydropower project. Consequently, the majority of the flow observed at this location primarily originates from subsurface contributions. These patterns are consistent with a combined influence of urban drainage, agricultural return flows, and baseflow transport of solutes and nutrients during the post-monsoon low-flow period. Accordingly, the upper Ganga displays a hydrochemical duality: monsoon conditions emphasize dilution and downstream mixing, whereas post-monsoon conditions accentuate geogenic weathering contributions and increase the detectability of human-derived inputs[26]. Sediment provenance, from the Himalayan orogen, the alluvial plains, and cratonic sources[15,30], may further regulate ionic balance via mineral dissolution and surface-sorption processes, reinforcing spatial differences in solute acquisition. Overall, geology and hydrology establish the baseline framework upon which seasonal forcing and anthropogenic pressures are subsequently expressed in river chemistry.

Seasonal hydrochemical facies transitions

Piper diagrams (Fig. 2i) show a clear seasonal duality. During the monsoon, waters are dominated by HCO_3^-–Ca^{2+}–Mg^{2+} facies, reflecting carbonate-buffered alkalinity and alkaline-earth cations under conditions of strong hydrological flushing and dilution by rainfall and meltwater contributions. This facies reflects (i) rapid throughflow with limited residence time, and (ii) sustained supply of HCO_3^- and Ca^{2+}–Mg^{2+} from carbonate-bearing lithologies and carbonate-rich metasediments. Overlapping on this baseline, a subtle downstream shift toward SO_4^{2-} water type suggests incremental inputs from atmospheric wet deposition during intense precipitation events and/or oxidative weathering of sulfide-bearing minerals, processes that can become more apparent as the river integrates progressively larger and more lithologically diverse catchment areas.

In the post-monsoon, facies evolve toward HCO_3^-–SO_4^{2-}–Ca^{2+}–Mg^{2+}, consistent with reduced discharge, longer residence times, and a larger proportional contribution from groundwater. This transition implies enhanced water–rock interaction, including sulfate generation through continued sulfide oxidation and/or

dissolution of sulfate-bearing phases, coupled with sustained carbonate buffering. Importantly, samples from Haridwar exhibited a more distinct Na^+–Cl^- enrichment, a pattern that is difficult to explain by lithology alone and instead points to increased influence of (i) groundwater mixing along the alluvial corridor, (ii) cation exchange processes that can elevate Na^+ relative to Ca^{2+}–Mg^{2+} in longer-residence waters, and (iii) anthropogenic sources such as wastewater inputs and urban runoff, which are more detectable when dilution capacity is lowest. The box plots (Fig. 2ii) confirm these interpretations by showing systematically higher ionic concentrations during post-monsoon despite reduced discharge, reflecting concentration effects and enhanced subsurface contributions.

Geochemical ratios and anthropogenic imprints

Bivariate ratios provide a process-level separation of solute sources and emphasized the seasonal shift from dilution-driven to baseflow-amplified hydrochemistry (Fig. 3). During the monsoon, scatter in NO_3^--K^+ and NO_3^--Cl^- relations (Fig. 3i) is consistent with diffuse and temporally variable inputs arising from fertilizer leaching, rapid surface runoff, and sewage flushing under high-flow conditions. In this period, anthropogenic tracers are present but are frequently masked by dilution and short residence times, resulting in weak coherence among nutrient-related ions. The TDS vs. $(NO_3^-+ Cl^-)/HCO_3^-$ ratios (Fig. 3ii) further indicate that the anthropogenic inputs are superimposed on carbonate weathering. In post-monsoon, several relationships are markedly tighter and more interpretable, reflecting the emergence of structured controls under low discharge. The coherence in Ca^{2+}+Mg^{2+} vs. TZ^+ (Fig. 3i), HCO_3^-vs. Ca^{2+} (Fig. 3i), and Na^+ vs. Cl^- (Fig. 3i) is consistent with (i) stronger baseflow buffering of river chemistry, (ii) enhanced water-rock interaction (notably carbonate dissolution), and (iii) increasing relevance of ion exchange and wastewater-related inputs in downstream and urban-influenced reaches. The Cl^- vs. NO_3^-/ Cl^- ratios (Fig. 3ii) provide an additional constraint, helping to distinguish settings dominated by agricultural sources (elevated NO_3^- relative to Cl^-) from those influenced more strongly by wastewater/urban drainage (higher Cl^- and a reduced NO_3^-/Cl^- ratio). Seasonal contrasts in major anion behavior reinforce this transition. Monsoon chemistry is dominated by conservative, dilution-controlled patterns, whereas post-monsoon samples display coherent NO_3^-–K^+–Cl^- associations that point to a mixture of sewage inputs, fertilizer residues, urban runoff, and atmospheric contributions (e.g., biomass-burning aerosols). These observations are consistent with findings from the eastern Himalayas, where arsenic and PAHs illustrate both local contamination and long-range atmospheric deposition[31,32].

Isotopic dynamics and seasonal clustering pathways

Stable isotopes ($\delta^{18}O$ and δD) exhibit marked seasonal differences (Fig. 4i), providing an independent constraint on hydrological processes that complements major-ion evidence. During the monsoon, isotopes define a meteoric-like relationship indicative of rainfall dominance and rapid mixing that homogenizes both chemical and isotopic signals. In contrast, post-monsoon samples show subtle enrichment and slope modification, consistent with evaporative effects and longer residence times under reduced discharge conditions. The altitude dependence of $\delta^{18}O$ (Fig. 4i.c–d) further confirms the influence of orographic depletion and glacial inputs. In both seasons, $\delta^{18}O$ exhibits a clear lapse rate, with more depleted values at higher elevations and progressive enrichment downstream. Local deviations from this gradient reflect tributary inputs during monsoon peak flow and enhanced baseflow mixing during post-monsoon recession.

The relationship between d-excess and $\delta^{18}O$ (Fig. 4i.e) reveals a clear seasonal separation. Monsoon samples are characterized by depleted $\delta^{18}O$ values and relatively higher d-excess, consistent with rapid meteoric recharge and limited evaporative modification. In contrast, post-monsoon samples shift toward enriched $\delta^{18}O$ values accompanied by reduced d-excess, indicating enhanced evaporation and longer effective residence times under low-flow conditions. The coupling between d-excess and Cl^- (Fig. 4i.f) further clarifies the role of conservative solute enrichment. Monsoon samples display greater scatter, reflecting diffuse runoff and rapid mixing that dilute both isotopic and chemical signatures. Post-monsoon samples, however, cluster toward lower d-excess values with elevated Cl^- concentrations, indicating that isotopic modification occurs alongside conservative solute accumulation. This pattern suggests that evaporation and anthropogenic inputs become increasingly visible when dilution capacity declines. A similar inverse relationship between d-excess and TDS (Fig. 4i.g,h) reinforces this interpretation. Increasing TDS during post-monsoon is accompanied by declining d-excess, demonstrating that isotopic modification and bulk solute concentration evolve in tandem during recession flow. Moreover, isotopic correlations with HCO_3^- and NO_3^- (Fig. 4i.i–l)) highlight seasonal nutrient–water coupling: diffuse surface runoff dominates during monsoon, while subsurface processes govern post-monsoon.

Hierarchical clustering further reveals seasonal restructuring of isotopic controls (Fig. 5i). During the post-monsoon, isotopes follow a sequential clustering pathway: initially with pH, subsequently with TSS, and finally with the broader ionic consortium (Fig. 5i). The initial linkage with pH suggests that, during low-flow conditions, carbonate equilibria and CO_2 exchange exert a rapid buffering effect on river water chemistry while isotopic composition begins to reflect longer residence pathways. Subsequent association with TSS is consistent with stronger sediment–water interactions during reduced flows, when fine particles and reactive surfaces can modulate both solute behaviour and the apparent co-variation among parameters. Final integration with major ions marks increasing groundwater/baseflow integration, consistent with longer residence times, which governs the major-ion signature under post-monsoon recession flow conditions. Together, this sequential clustering pathway is process-informative, reflecting a progression from rapid buffering (pH) to sediment mediation (TSS) and finally to integrated subsurface control.

To separate these controls, we interpret the isotope patterns using three complementary constraints: (i) δD–$\delta^{18}O$ slope behavior (Fig. 4i), (ii) integrated d-excess relationships with conservative solutes, (iii) clustering relationships among isotopes and hydrochemical variables (Fig. 5i) combined with site-specific setting (reservoir reaches, tributary junctions, and urban/pilgrimage corridors). Localized isotopic anomalies that co-occur with strong ionic coherence (e.g., EC–Cl^- and EC–NO_3^-) and post-monsoon clustering behavior (e.g., G20) are

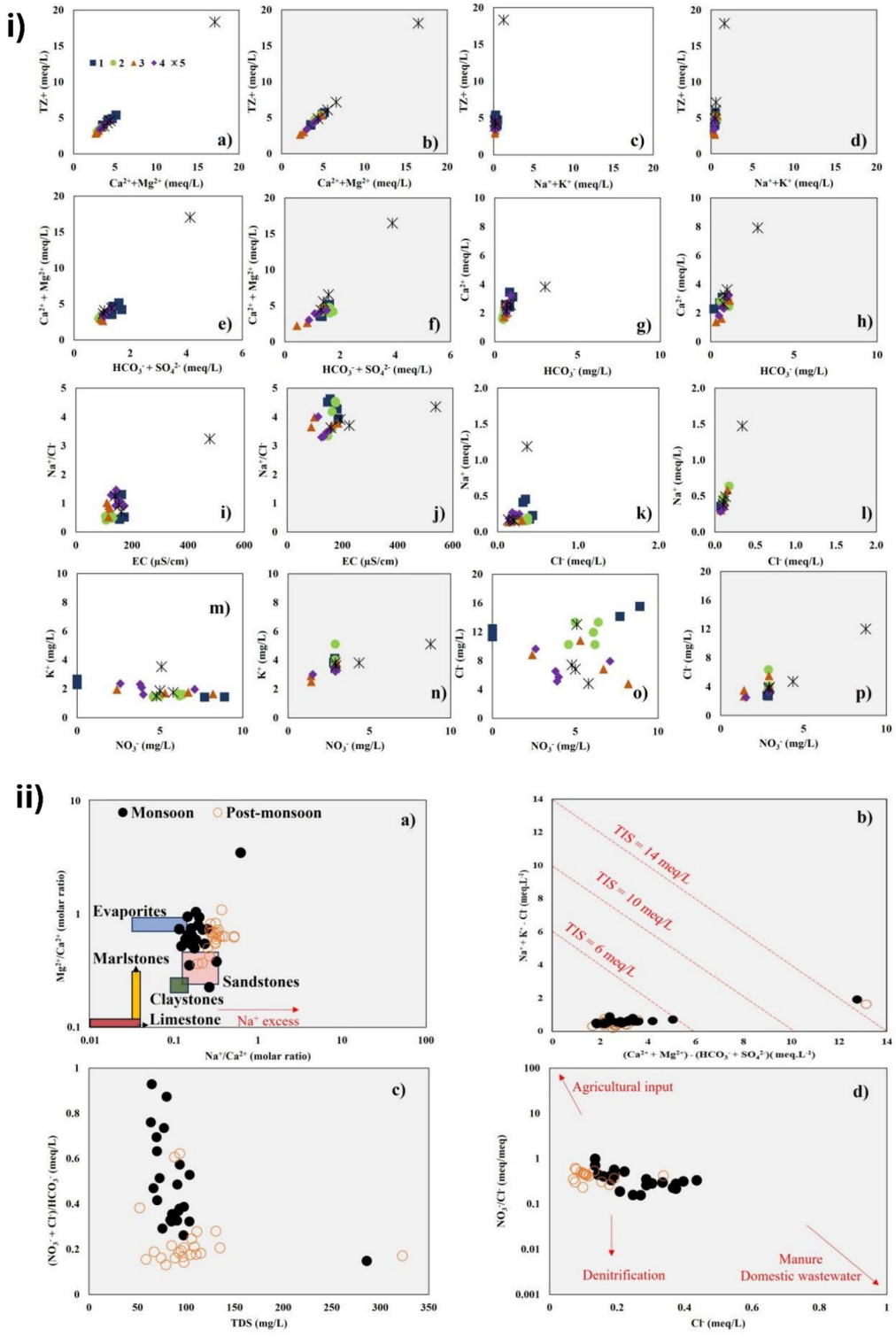

Fig. 3. Decoding geochemical controls and processes illustrating dilution- and baseflow-controlled regimes. (**i**) Bivariate relationships among major cations and anions. Grey-shaded & transparent panels (**i**a-p) represent post-monsoon and monsoon samples, respectively. (**ii**) Diagnostic scatter plots dominant processes: (a) Na/Ca vs. Mg/Ca, (b) Ion-exchange index, (c) TDS vs. $(NO_3^-+Cl^-)/HCO_3^-$, (d) Cl^- vs. NO_3^-/Cl^-.

interpreted as groundwater/hyporheic inflow and longer residence-time mixing. Anthropogenic pollution is inferred primarily from conservative tracers (NO_3^-, Cl^-, K^+) and spatial coincidence with impacted reaches; isotopes mainly constrain the hydrological pathways (mixing, residence time, evaporation) through which these solutes are expressed.

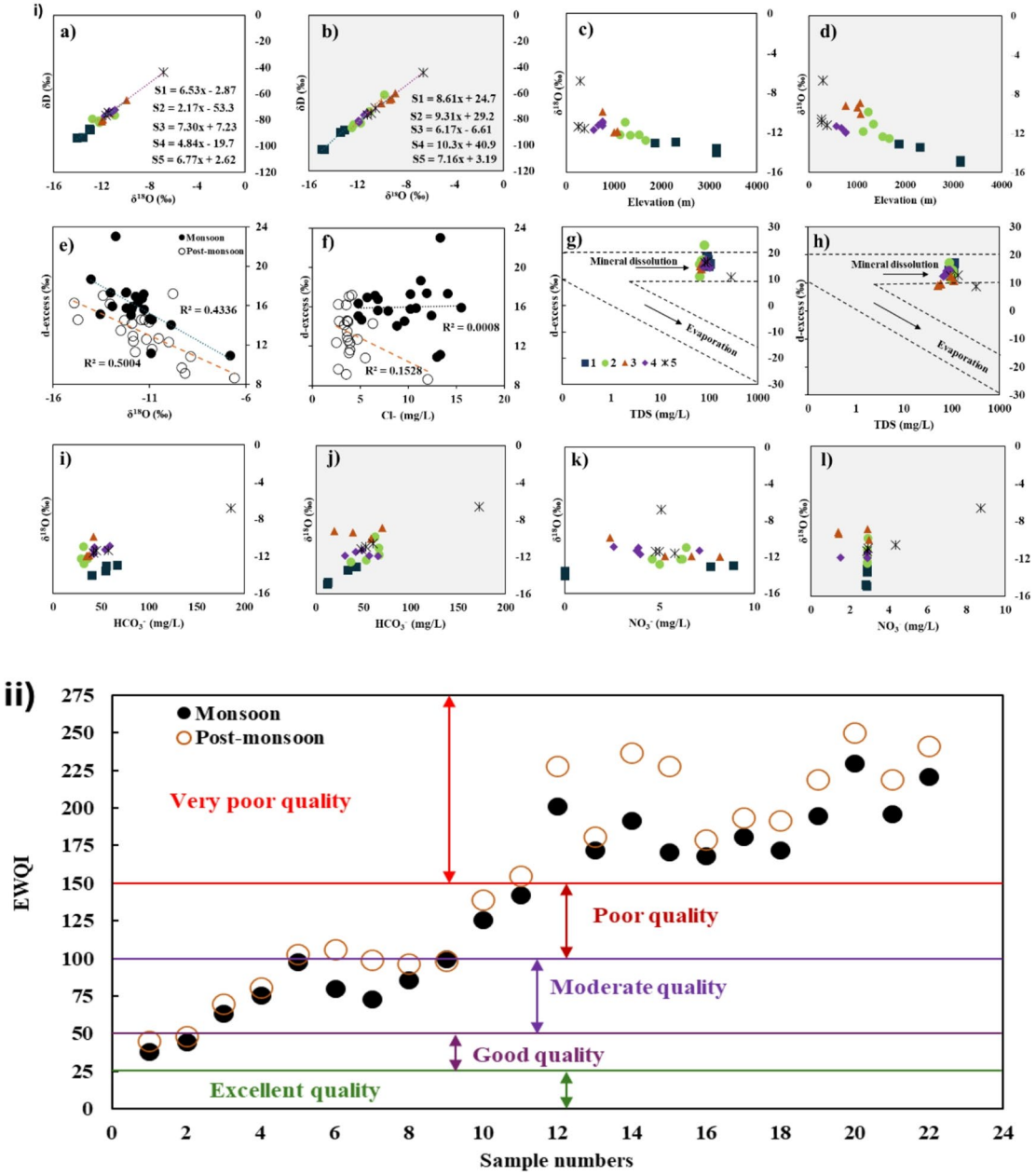

Fig. 4. Stable isotope process diagnostics and seasonal water quality assessment. In (e–f), monsoon samples are solid circles and post-monsoon are hollow circle while from (a-d, g–l), monsoon panels have transparent backgrounds and post-monsoon panels are grey-shaded. (**i**) (a–b) $\delta^{18}O$–δD relationships with altitude effects, (c–d) $\delta^{18}O$ versus elevation illustrating systematic depletion upstream, e) d-excess versus $\delta^{18}O$ illustrating evaporative modification and moisture source variability, (f) d-excess versus Cl^- indicating evaporation-driven solute enrichment, (g-h) d-excess versus TDS for highlighting seasonal evaporative concentration effects, (i–l) Coupling of $\delta^{18}O$ with HCO_3^- and NO_3^- highlighting anthropogenic imprints. (**ii**) EWQI values for monsoon and post-monsoon samples.

Altitude and tributary influences

In both seasons, $\delta^{18}O$ shows a clear altitude control, with lapse rates of ~ − 0.13‰/100 m in monsoon and ~ − 0.17‰/100 m in post-monsoon, consistent with orographic depletion and broadly aligned with previous Himalayan observations[33]. In addition to this regional gradient, local deviations highlight tributary and glacier-melt effects. For example, $\delta^{18}O$ values become more depleted from G1 to G2 (− 13.5 to − 14.1‰ monsoon; −14.7 to − 14.9‰ post-monsoon) due to Kedartaal glacier inputs. Further depletion between G3–G4 during monsoon suggests tributary contributions (e.g., Jadh Ganga) during peak-flow conditions. Post-monsoon, these reaches are slightly enriched, indicating reduced glacial contribution and greater baseflow mixing.

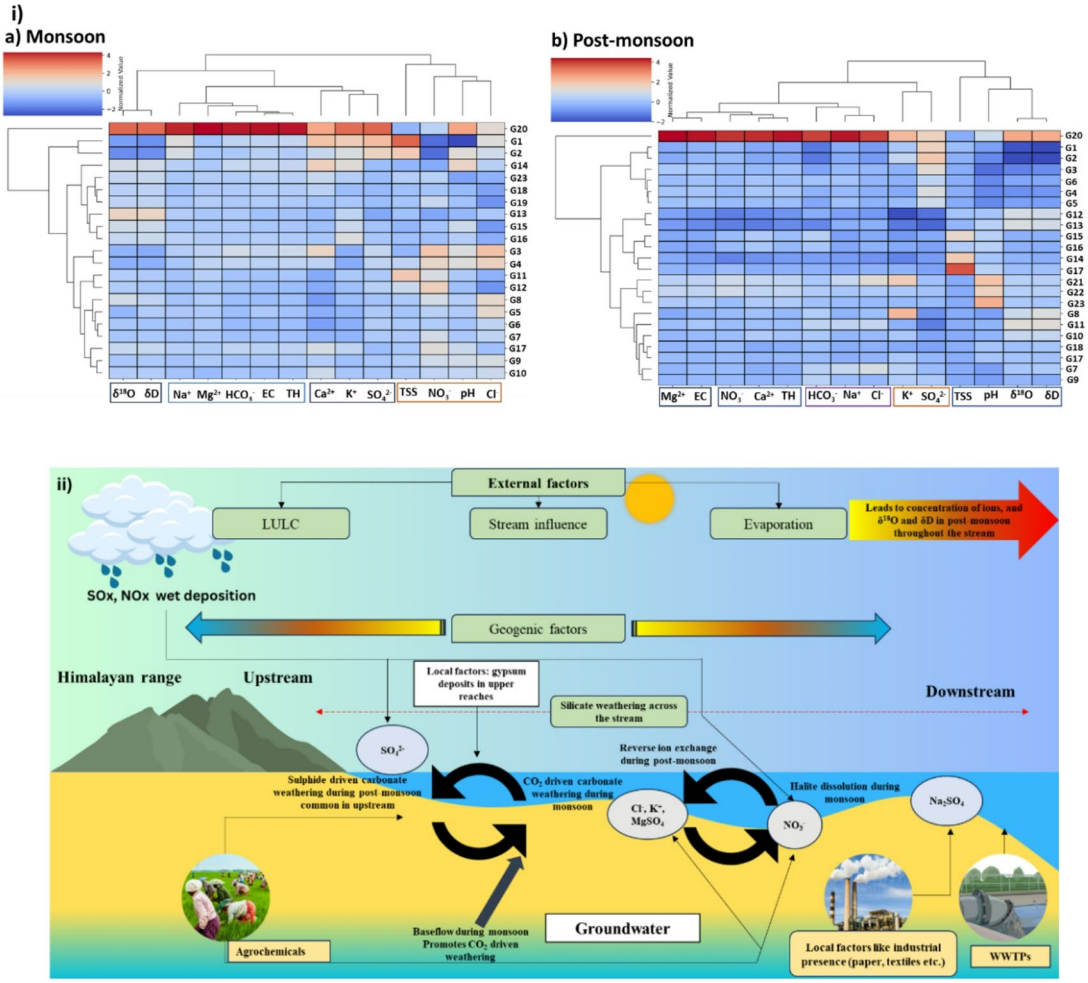

Fig. 5. Heatmap clustering and conceptual synthesis of seasonal hydrochemical controls. (**i**) Heatmap with Q-mode and R-mode hierarchical clustering. (a) Monsoon sites cluster into glacier-fed headwaters, whereas (b) post-monsoon clusters separate into upstream glacier-fed and solute-enriched midstream/downstream groups. (**ii**) Conceptual model summarizing seasonal controls on hydrochemistry and anthropogenic imprinting along the upper Ganga River.

Reservoir and evaporation modification

At Tehri (G13), isotopic enrichment ($\delta^{18}O \approx -10‰$ vs. $\sim -12‰$ upstream) combined with deviation from the LMWL (Fig. 4i) indicates reservoir-induced evaporation. A smaller enrichment near Uttarkashi (G8), followed by re-depletion at G9, reflects sluggish reaches and subsequent mixing. These isotopic enrichments coincide with higher TDS and excess $Ca^{2+}+Mg^{2+}$ relative to $HCO_3^-+SO_4^{2-}$ (Fig. 3i), suggesting that reservoir storage enhances both evaporation-driven isotopic fractionation and solute accumulation.

Groundwater and subsurface inputs

Saptrishi Ashram (G20) shows a marked isotopic anomaly, with $\delta^{18}O$ values enriched to $\sim -6.8‰$ in monsoon and $-6.6‰$ in post-monsoon, compared with ~ -11 to $-12‰$ at adjacent sites. This localized enrichment, together with strong post-monsoon ionic coherence ($EC–Cl^-$ and $EC–NO_3^-$, $r > 0.9$; Fig. 2iv) and the site's clustering behavior (Fig. 5i), supports groundwater inflow and/or hyporheic exchange as the dominant control rather than reservoir evaporation. Downstream, $\delta^{18}O$ values return to depleted levels at G21–G22, confirming mixing with glacially sourced flows.

Hydropower diversion impacts

Hydropower operations further modulate isotopic variability by imposing storage, diversion, and re-mixing along the river corridor. At G20, diversion and temporary storage enhance evaporative enrichment, while rejoining at Bhim Gowda Barrage (G21) lowers $\delta^{18}O$ to $\sim -10.5‰$, evidencing dilution and re-mixing. These engineered structures, therefore, imprint isotopic signals primarily by altering residence time and promoting localized evaporation/mixing, rather than by directly changing isotope ratios through pollutant inputs; this distinction is important when interpreting anthropogenic influence in regulated Himalayan rivers.

Seasonal synthesis of isotopic controls

Collectively, isotopic evidence delineates two contrasting seasonal regimes. During the monsoon, river isotopes are dominated by meteoric inputs and rapid mixing, producing homogenized compositions aligned with the LMWL and obscuring localized influences. In contrast, post-monsoon baseflow conditions reintroduce spatial and process-specific controls, allowing evaporation, groundwater inflow, and flow regulation to be resolved through isotopic slopes, clustering behavior, and site-specific anomalies. This seasonal duality highlights the value of isotopes as integrative tracers of both hydrological processes and human modification in Himalayan river systems.

Correlation networks and multivariate analyses

Pearson correlation matrices (Fig. 2iv and Fig. S3) reveal restructuring of chemical networks. During the monsoon, weak associations between nutrients (NO_3^-, K^+, Cl^-) and major ions suggest surface flushing and diffuse runoff. In post-monsoon, strong positive correlations emerge among Ca^{2+}, Mg^{2+}, HCO_3^-, SO_4^{2-}, EC, and TH ($r > 0.8$), consistent with carbonate–silicate weathering dominance under baseflow. Principal component analysis (Table S3) confirms this seasonal shift. In the monsoon, PC2 loads on TSS and NO_3^-, emphasizing episodic inputs. In contrast, post-monsoon PC1 is dominated by ionic parameters, indicating geogenic structuring. NO_3^- transitions from a surface-driven signal in monsoon to subsurface transport in post-monsoon, underscoring its mobility and seasonal persistence.

Hierarchical clustering (Q-mode and R-mode) (Fig. 5i) with associated heat maps effectively complements PCA by elucidating groupings among both hydrochemical parameters and sampling sites, thereby enhancing interpretations of seasonal hydrogeochemical dynamics. As evidenced in Fig. S4, Q-mode analysis of monsoon samples delineates three distinct site groups: glacier- and snowmelt-dominated headwaters (G1–G2) with depleted isotopes and minimal EC/TH; mainstream sites (G3–G19) with diluted HCO_3^-–Ca^{2+}–Mg^{2+} chemistry indicative of peak-flow conditions; and the outlier Saptrishi Ashram (G20), characterized by high Na^+, K^+, SO_4^{2-}, and HCO_3^- concentrations, which reflect localized groundwater inputs and anthropogenic impact. Post-monsoon clustering retains this tripartite structure, but with greater intergroup contrast: upstream sites (G1–G6) remain low in salinity and isotopically depleted, while mid- to downstream segments (G7–G19, G21–G22) show higher solute accumulation due to extended residence time and intensified groundwater contributions. G20 continues as a solute-rich outlier, highlighting persistent baseflow influence and anthropogenic loading. Heat maps reinforce these spatial distinctions, especially the persistent extremity of G20 and the downstream increase in solutes after rainfall. R-mode clustering of variables also exhibits seasonal reorganization; during the monsoon, isotopic variables ($\delta^{18}O$, δD) form a branch distinct from chemical clusters, signifying the overriding influence of altitude and meteoric input, whereas geogenic ions cluster separately, and an anthropogenic branch (pH–Cl^-– NO_3^-–TSS) suggests storm-driven pollution and sediment transport. Post-monsoon, isotopic variables cluster with pH and TSS, implicating increasing control by evaporation, buffering, and sediment–solute dynamics, while Mg^{2+} aligns closely with EC, implying greater groundwater modulation of salinity.

Entropy water quality index and the physics of disorder

Entropy-based approaches are particularly well suited to Himalayan river systems, where extreme seasonality, steep topographic gradients, and rapid shifts between high-flow and baseflow conditions generate nonlinear water-quality responses. Traditional indices such as WQI or NSFWQI rely on fixed parameter weights and threshold-based scoring, which can mask diffuse degradation during high-flow dilution[27,28]. In contrast, EWQI derives parameter weights from information entropy calculated from the normalized dataset, so weights reflect the relative informational contribution of each parameter under the observed hydroclimatic conditions. This makes EWQI sensitive to cumulative, low-intensity anthropogenic pressures characteristic of glacier-fed, monsoon-influenced river systems. EWQI provides system-level insight that complements facies-based hydrochemical interpretation. While major ions and facies diagrams effectively resolve dominant geogenic processes and seasonal dilution, EWQI captures multivariate disturbance as an integrated signal of disorder.

EWQI scores (Fig. 5i) show significant deterioration: ~50% of monsoon and 54% of post-monsoon samples fall into the "very poor" category (mainly downstream). Only ~ 9% of samples in both seasons (all upstream) qualify as "good." Importantly, EWQI values rise from monsoon to post-monsoon, reflecting not only the concentration of solutes under low flow but also the persistence of anthropogenic perturbations when dilution ceases. For instance, G1, a headwater site, remained "good" but worsened from 38.13 to 45.15, while G23 deteriorated further from 251.56 to 267.25. Seasonal contrasts, therefore, reflect a "physics of disorder," where monsoon flows partly reset conditions through dilution and flushing, whereas post-monsoon recession reveals accumulated perturbations from solutes and suspended matter[27,28].

The dataset analyzed here was collected during monsoon and post-monsoon 2015 and therefore represents conditions during the sampled period. No contemporary spot-check sampling was conducted as part of this study. Accordingly, we do not interpret the results as a direct assessment of present-day (2024/2025) water quality status or trends. Instead, the key contribution is a process-based interpretation of seasonal hydrogeochemical–isotopic dynamics along a headwater-to-foothill transect, including dilution versus baseflow regimes, mixing behavior, isotopic clustering responses, and the complementary diagnostic value of EWQI. Future work should evaluate how the magnitude of these signals has evolved under recent changes in infrastructure, land use, and hydroclimate.

Conceptual synthesis: from pristine to anthropocene rivers

The conceptual schematic (Fig. 5ii) integrates hydrogeochemical, isotopic, and statistical findings to delineate seasonal controls on water chemistry in the upper Ganga. Natural drivers (weathering, dissolution, ion exchange) form the hydrogeochemical backbone, most pronounced in baseflow. During the monsoon, rapid flow enhances

carbonate dissolution but dilutes most solutes, and promotes sulfide oxidation due to hillslope runoff, resulting in HCO_3^-–Ca^{2+}–Mg^{2+} dominant signature. Atmospheric deposition (including biomass-burning aerosols) is quickly diluted, while isotopic and TSS data reveal altitude and sediment contributions. Post-monsoon, reduced flow increases groundwater impact and water–rock interaction, enriching solutes such as Cl^-, NO_3^-, and SO_4^{2-} from both natural and anthropogenic sources, with distinct ion correlations highlighting sewage and runoff inputs. Localized isotopic enrichment in sites like Tehri Reservoir reflects additional evaporation and human impacts. EWQI results confirm a shift to poorer water quality downstream in the post-monsoon, with cluster analyses distinguishing geogenic from recurrent anthropogenic hotspots, notably at site G20.

Summarily, anthropogenic drivers like fertilizers, sewage, atmospheric deposition, overlay this framework, mediated by monsoon hydrology. Importantly, this influence is not confined to downstream urban reaches. The uppermost headwater sites (G1–G4), including the Gangotri glacial corridor, exhibit detectable NO_3^- concentrations (up to 8.9 mg/L), non-zero Cl^- levels, and subtle isotopic deviations from purely meteoric–melt mixing at select locations. This synthesis underscores a paradox: the Ganga headwaters, long perceived as pristine, are already imprinted by human influence within the hydrological source zones of the basin. While these signals remain modest relative to downstream sites, they amplify through cumulative wastewater inputs, groundwater interaction, and localized evaporation, culminating in degraded water quality reflected by post-monsoon EWQI deterioration and anthropogenic clustering at sites such as G20. Overall, isotopes constrain meltwater–meteoric mixing and evaporation, whereas ion patterns and multivariate structure indicate superimposed anthropogenic inputs, consistent with mountain rivers acting as early-warning sentinels of Anthropocene transformation[18,29].

Implications for sustainability and governance

Three key lessons emerge: (i) Monitoring blind spots: monsoon-only monitoring underestimates persistent anthropogenic influence because high flows dilute and homogenize signals; post-monsoon observations are therefore essential. (ii) Entropy as a diagnostic: framing water quality as entropy highlights system-wide disorder and cumulative disturbance, emphasizes resilience as a dynamic reorganization capacity, rather than compliance with static thresholds. (iii) Policy linkages: protecting Himalayan headwaters is essential for achieving SDG 6 and SDG 13, requiring adaptive governance that integrates hydrological seasonality, land use pressures, and long-range pollutant transport. The uppermost headwaters are not interpreted as severely degraded. The paradox lies in the detectable embedding of anthropogenic signals within reaches commonly assumed to be pristine baselines, while the magnitude and coherence of these signals increase downstream and during post-monsoon low-flow conditions when dilution capacity is lowest. Thus, the upper Ganga exemplifies the global sustainability paradox for glacier-fed rivers: systems treated as "pristine" in governance narratives can already carry embedded human signatures, demanding monitoring and management approaches that bridge hydrochemistry, isotope hydrology, and sustainability science.

Conclusion

This study of the upper Ganga River reveals a striking paradox: one of the world's most venerated and ostensibly pristine Himalayan headwaters is already structurally embedded in the Anthropocene water cycle. Across seasons, hydrochemical facies, isotopic signatures, and entropy-based diagnostics show that natural geogenic structuring coexist with persistent anthropogenic imprinting, even at high elevations. Seasonal hydrology modulates the visibility of these signals, with monsoon dilution masking chronic pressures that re-emerge under post-monsoon low-flow conditions. By integrating entropy-based assessment with conventional hydrochemical and isotopic tools, this work advances river science beyond concentration-based thresholds toward a system-level perspective on disorder and resilience. The entropy framework is particularly effective in revealing subtle but persistent deterioration that may remain undetected in facies-based or single-parameter analyses, especially in headwater reaches that retain apparently natural chemistry.

These insights carry urgent policy implications for sustainability and governance. Climate change is expected to intensify monsoon extremes, accelerate glacial retreat, and alter baseflow regimes, amplifying the very dynamics documented here. For governance, this means that protecting Himalayan headwaters requires adaptive monitoring, seasonal sensitivity, and recognition of long-range pollutant transport. More fundamentally, it demands a shift from treating pristine headwaters as invulnerable natural sources to recognizing them as early-warning sentinels of Anthropocene transformation.

Materials and methods

Study area

The study covers the 255 km stretch of the upper Ganga from Gangotri (3143 m) to Haridwar (262 m). This region traverses glaciers, metamorphic and carbonate terrains, and pilgrimage towns before entering the North Indian plains. Hydrological seasonality is pronounced. The study area spans a diverse landscape that transitions from the rugged terrains of the Himalayas to the fertile plains of Uttarakhand. This stretch is crucial as it represents the early journey of the river where it begins to accumulate various inputs from tributaries and human activities before it traverses the more densely populated and industrialized regions downstream[16,29]. The Ganga River originates as the Bhagirathi River (one of its headstreams) from Gaumukh (30° 36′ N; 79° 04′ E), in the Gangotri glacier at an elevation of around 4000 m above mean sea level (amsl) (Singh et al., 2007). This region is characterized by a harsh climate and a fragile ecosystem, sensitive to the impacts of climate change and human activities[18]. As the river descends, it encounters various small towns and pilgrimage sites, accumulating inputs from both natural and anthropogenic sources. The hydrology of this region is markedly influenced by the monsoon patterns, which can dramatically alter the river's flow and sediment load, influencing water quality and availability.

Upon reaching Haridwar, the Ganga exits the mountainous terrain and enters the North Indian plains. Haridwar holds immense religious significance and attracts millions of pilgrims and tourists annually, which presents unique challenges such as increased water extraction and pollution load. This area is a critical point of transition where the river's characteristics begin to change markedly, influenced by agricultural runoff, industrial waste, and urban sewage. The study of this upper stretch of the Ganga is essential for understanding the early alterations in the river's chemistry and flow dynamics, setting the stage for all downstream analysis. By capturing and analysing water samples from this varied and dynamic region during different seasonal flows, we aim to characterize the seasonal hydrogeochemical and isotopic processes operating along this headwater-to-foothill transect during the sampled period, and to interpret how geogenic structuring and anthropogenic imprinting vary between monsoon and post-monsoon conditions.

Sampling and analysis

Fifty samples from 25 sites were collected in the monsoon (June) and post-monsoon (November) 2015. The study is designed to resolve seasonal process contrasts along a spatial transect. It does not assess temporal trends to the present, and no contemporary spot-check sampling was undertaken. Parameters measured included pH, EC, TDS, TH, TSS, major ions (Ca^{2+}, Mg^{2+}, Na^{+}, K^{+}, Cl^{-}, SO_4^{2-}, HCO_3^{-}, NO_3^{-}), and stable isotopes (δD, $\delta^{18}O$). Physicochemical parameters were measured in-situ using a portable multiparameter (HACH HQ40-D, USA), and coordinates were recorded. Samples were collected in pre-cleaned polyethylene bottles and filtered in the field by 0.45 µm filter paper. Filtered samples intended for cation analysis were acidified to pH < 2 with ultrapure nitric acid (HNO_3), whereas samples for major anion analysis were not chemically preserved. All samples were stored at 4 °C to minimize biological activity and transported to the laboratory at the National Institute of Hydrology Roorkee (NIH, Roorkee), India, for further analysis. Major ions were analyzed using Metrohm 930 IC, isotopes using continuous flow isotope ratio mass spectrometry (IRMS), and bicarbonates via potentiometric titration. Charge balance errors were within ± 5%.

Statistical and entropy analysis

Statistical Package for Social Science (IBM-SPSS) V.20 software was used for principal components analysis (PCA) and hierarchical cluster analysis (HCA). These were utilized to comprehend the complex interrelationships among different variables. Prior standardization of the data via z-score calculation was done, with further orthogonal transformation and varimax rotation for PCA[34]. We selected the principal components (PCs) with eigenvalues > 1. For classification of the data via HCA, the distance was analyzed using the Euclidean distance method and Ward's method for further linkage construction. Piper diagrams, correlation matrices, PCA, and bivariate plots were used to interpret hydrochemical patterns. Cluster analysis revealed grouping of isotopes and ions across seasons. EWQI was computed using entropy-based weights to integrate multiple parameters into a composite water quality index[27,28].

Isotope analysis

The surface water samples were analysed for δD and $\delta^{18}O$ at the laboratory of NIH, Roorkee, using IRMS with automated sample preparation. For $\delta^{18}O$, aliquots of water (~ 400 µL) were equilibrated with CO_2 gas at 40 °C for ~ 7 h, whereas for δD, aliquots (~ 400 µL) were equilibrated with H_2 gas in the presence of a Pt catalyst at 40 °C for ~ 3 h. The equilibrated gases were introduced into the IRMS to determine $^{18}O/^{16}O$ and $^{2}H/^{1}H$ ratios, from which $\delta^{18}O$ and δD values were calculated. The isotopic compositions were reported in delta notations (δ,‰) relative to Vienna Standard Mean Ocean Water (VSMOW) according to Eq. (1):

$$\delta = \left(\frac{R_{sample}}{R_{standard}} - 1\right) \times 1000 \quad (1)$$

where R represents the ratio of heavy to light isotopes ($^{2}H/^{1}H$ for δD and $^{18}O/^{16}O$ for $\delta^{18}O$) and $R_{standard}$ corresponds to VSMOW. Each sample was analyzed in triplicate, and mean values are reported. Analytical precision (1σ), evaluated from repeated measurements of laboratory standards, was ± 0.1‰ for $\delta^{18}O$ and ± 1.0‰ for δD.

Data availability

The dataset used and/or analysed during the current study is available from the corresponding author on reasonable request.

Received: 23 October 2025; Accepted: 10 March 2026
Published online: 19 March 2026

References

1. Meybeck, M. Global analysis of river systems: from Earth system controls to Anthropocene syndromes. *Philos. Trans. R Soc. Lond. B.* **358**, 1935–1955 (2003).
2. Vörösmarty, C. J. et al. Global threats to human water security and river biodiversity. *Nature* **467**, 555–561 (2010).
3. Islam, S. T. et al. State of the World's Rivers. *Annu. Rev. Environ. Resour.* **49**, 137–162 (2024).
4. Kumar, M., Ramanathan, A. & Keshari, A. K. Understanding the extent of interactions between groundwater and surface water through major ion chemistry and multivariate statistical techniques. *Hydrol. Process.* **23**, 297–310 (2009).
5. Kumar, M., Goswami, R., Awasthi, N. & Das, R. Provenance and fate of trace and rare earth elements in the sediment-aquifers systems of Majuli River Island, India. *Chemosphere* **237**, 124477 (2019).
6. Das, N., Das, A., Sarma, K. P. & Kumar, M. Provenance, prevalence and health perspective of co-occurrences of arsenic, fluoride and uranium in the aquifers of the Brahmaputra River floodplain. *Chemosphere* **194**, 755–772 (2018).

7. Gaillardet, J., Calmels, D., Romero-Mujalli, G., Zakharova, E. & Hartmann, J. Global climate control on carbonate weathering intensity. *Chem. Geol.* **527**, 118762 (2019).
8. Li, D. et al. The competing controls of glaciers, precipitation, and vegetation on high-mountain fluvial sediment yields. *Sci. Adv.* **10**, eads6196 (2024).
9. Arya, A. R. & Santhanam, H. Mapping the ecological worth of glaciers of the Indian Himalayan region. *Ecol. Ind.* **178**, 113917 (2025).
10. Pandit, M. K., Manish, K. & Koh, L. P. Dancing on the roof of the world: ecological transformation of the himalayan landscape. *BioScience*. **64**, 980–992 (2014).
11. Kumar, M., Panday, D. P., Bhagat, C., Herbha, N. & Agarwal, V. Demystifying the decadal shift in the extent of groundwater in the coastal aquifers of Gujarat, India: A case of reduced extent but increased magnitude of seawater intrusion. *Sci. Total Environ.* **898**, 165451 (2023).
12. Remya, S. N. et al. A framework to identify rock glaciers and model mountain permafrost in the Jhelum Basin, Kashmir Himalaya, India. *Earth Space Sci.* **11**, e2023EA003170 (2024).
13. Mishra, V., Malik, K., Agarwal, V., Mishra, P. K. & Jain, K. Impact assessment of unsustainable airport development in the Himalayas using remote sensing: A case study of Pakyong Airport, Sikkim, India. *Quat. Sci. Adv.* **13**, 100144 (2024).
14. Singh, R. & Singh, G. S. Integrated management of the Ganga River: An ecohydrological approach. *Ecohydrol. Hydrobiol.* **20**, 153–174 (2020).
15. Singh, M., Singh, I. B. & Müller, G. Sediment characteristics and transportation dynamics of the Ganga River. *Geomorphology* **86**, 144–175 (2007).
16. Matta, G., Kumar, A., Nayak, A. & Kumar, P. Appraisal of spatial–temporal variation and pollution source estimation of Ganga River system through pollution indices and environmetrics in Upper Ganga basin. *Appl. Water Sci.* **12**, 33 (2022).
17. Mukherjee, A. et al. Contesting with the Ganges Water Machine in South Asia: Theory versus Reality. *ACS EST. Water*. **3**, 626–628 (2023).
18. Prasad, S., Saluja, R., Joshi, V. & Garg, J. K. Heavy metal pollution in surface water of the Upper Ganga River, India: human health risk assessment. *Environ. Monit. Assess.* **192**, 742 (2020).
19. Pant, R. R. et al. Spatiotemporal variations of hydrogeochemistry and its controlling factors in the Gandaki River Basin, Central Himalaya Nepal. *Sci. Total Environ.* **622–623**, 770–782 (2018).
20. Tiwari, A., Joshi, S. K., Tripathi, S. K. & Saxena, R. Spatial pattern of groundwater recharge in Jhansi district in the Bundelkhand region, central India. *Environ. Dev. Sustain.* **23**, 18618–18630 (2021).
21. Jeelani, G. et al. Distinguishing and estimating recharge to karst springs in snow and glacier dominated mountainous basins of the western Himalaya, India. *J. Hydrol.* **550**, 239–252 (2017).
22. Craig, H. Isotopic variations in meteoric waters. *Science* **133**, 1702–1703 (1961).
23. Ansari, M. A. et al. Assessing the groundwater recharge processes in intensively irrigated regions: An approach combining isotope hydrology and machine learning. *Geosci. Front.* **16**, 102105 (2025).
24. Kedia, S., Vellore, R. K., Islam, S. & Kaginalkar, A. A study of Himalayan extreme rainfall events using WRF-Chem. *Meteorol. Atmos. Phys.* **131**, 1133–1143 (2019).
25. Boral, S. & Sen, I. S. Tracing 'Third Pole' ice meltwater contribution to the Himalayan rivers using oxygen and hydrogen isotopes. *Geochem. Persp. Lett*. 48–53. https://doi.org/10.7185/geochemlet.2013 (2020).
26. Trivedi, R. C. Water quality of the Ganga River—An overview. *Aquat. Ecosyst. Health Manag.* **13**, 347–351 (2010).
27. Amiri, V., Rezaei, M. & Sohrabi, N. Groundwater quality assessment using entropy weighted water quality index (EWQI) in Lenjanat, Iran. *Environ. Earth Sci.* **72**, 3479–3490 (2014).
28. Han, X., Tang, F. & Liu, A. L. Drinking water quality evaluation in supply systems in Wuhan, China: application of entropy weight water quality index and multivariate statistical analysis. *Environ. Sci. Pollut Res.* **31**, 280–292 (2023).
29. Matta, G., Nayak, A., Kumar, A. & Kumar, P. Water quality assessment using NSFWQI, OIP and multivariate techniques of Ganga River system, Uttarakhand, India. *Appl. Water Sci.* **10**, 206 (2020).
30. Pathak, S. S. & Mishra, P. A. Review of the Ganga River water pollution along major urban centers in the State of Uttar Pradesh, India. *IRJET* 07, (2020).
31. Deka, J. P. et al. Long-range transport of polycyclic aromatic hydrocarbons and metals in high altitude lacustrine environments of the Eastern Himalayas: Speciation, and source apportionment perspectives. *ACS EST. Water*. **4**, 3400–3411 (2024).
32. Ansari, M. A. et al. Isotope hydrology tools in the assessment of arsenic contamination in groundwater: An overview. *Chemosphere* **340**, 139898 (2023).
33. Khan, A. A. et al. The Himalayan cryosphere: A critical assessment and evaluation of glacial melt fraction in the Bhagirathi basin. *Geosci. Front.* **8**, 107–115 (2017).
34. Narvaez-Montoya, C., Mahlknecht, J., Torres-Martínez, J. A., Mora, A. & Bertrand, G. Seawater intrusion pattern recognition supported by unsupervised learning: A systematic review and application. *Sci. Total Environ.* **864**, 160933 (2023).

Acknowledgements

We would like to thank Dr. Durga Prasad Panday for adding valuable inputs to this article. All the analyses were made at NIH, Roorkee.

Author contributions

This article is co-authored by M.K. and S.T. as first authors. Conceptualization: M.K., R.S., and S.P.R.; Methodology: M.K., R.S., N.D., and J.A.T.M.; Investigation and analysis: R.S., SPR.; Data curation: S.T., and N.D.; Visualization: M.K., N.D., and S.T. Writing—original draft preparation: M.K. and S.T.; Writing—review and editing: R.S., S.P.R., N.D., V.A. , P.K.J., and J.A.T.M.; Supervision: M.K. All authors have read and agreed to the published version of the manuscript.

Funding

We thankfully acknowledge the financial assistance provided by the Department of Science and Technology, Government of India, under the DST grant. We would like to thank Tecnológico de Monterrey for the financial support; and NIH Roorkee for infrastructure support.

Declarations

Competing interests

The authors declare no competing interests.

Consent to participate
The authors consent to participate in this research study.

Consent to publish
The authors consent to publish this research study.

Additional information
Supplementary Information The online version contains supplementary material available at https://doi.org/10.1038/s41598-026-44251-8.

Correspondence and requests for materials should be addressed to M.K. or R.S.

Reprints and permissions information is available at www.nature.com/reprints.

Publisher's note Springer Nature remains neutral with regard to jurisdictional claims in published maps and institutional affiliations.